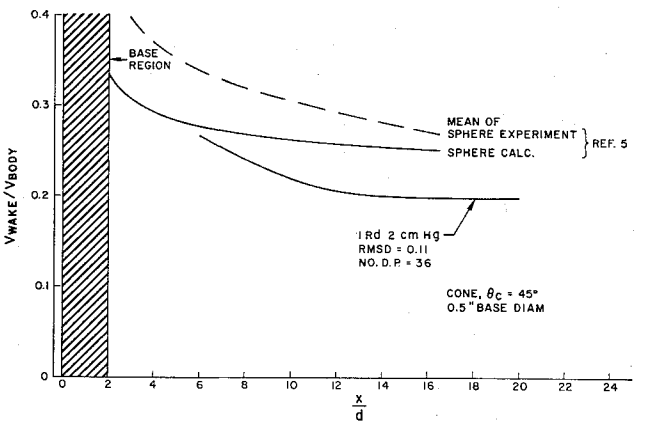

Fig. 5 Cone wake velocity data for a 45° semivertex angle cone; $d_{base} = \frac{1}{2}$ in., $p_\infty = 2$ cm Hg. Data compared with sphere wake results.

large-scale structure will not be sufficient to induce a turbulent growth of the wake, and a slower velocity decay tending toward the higher velocities of a theoretical laminar result is to be expected. Evidence of such an effect is somewhat suggested by the $P\infty = 0.88$ and 1-cm data in the experimental results presented in Fig. 4. It must be remembered that this suggestion is based mostly on a phenomenological expectation.

The unsteady wake phenomenon in the sphere experiments was observed as streaks in the same manner as just shown for the cone. However, the sphere calculation shown in Fig. 4 comes from an inviscid stream tube calculation. For spheres, the near-wake region $x/d < 15$ is dominated by the strong pressure decay. The large-scale unsteady structure in the viscous core is sucked into the expansion region, and consequently the velocity decay is being dominated by the pressure distribution set up by the shock-induced inviscid flow field rather than by turbulent diffusion.

A physical explanation as to why sphere wake velocities are higher than the cone wake velocities may be as follows. The sphere produces a relatively large-radius shock, thereby creating a large flux of high-velocity gas in and adjacent to the viscous core. In the slender cone case, $\theta_c \sim 15°$, the gas adjacent to the viscous core is of relatively low velocity (very nearly the ambient value) and hence more rapidly decelerates the viscous core gas via turbulent diffusion.

Experimental results for the 45° semivertex angle cone, $d_{base} = \frac{1}{2}$ in., do not fall along the slender cone theory line (Fig. 3) but come near to, although lower than, the sphere results (Fig. 5). The C_D shock drag for a 45° cone and for a sphere are approximately equal, both being close to one. However, the distribution of the momentum deposition in the gas behind the shock is somewhat different. In the sphere case, the deposition is nonuniform because of the large curvature of the bow shock. This gives rise to larger velocities at smaller radii and smaller velocities further out in the flow field. In the cone case, the shock is straight, the deposition is uniform, and the velocities at small radii are relatively less than those in the sphere case. Thus, in the case of the 45° cone relative to the sphere, the gas adjacent to the viscous core is of relatively lower velocity, hence decelerating the viscous core gases more rapidly via turbulent diffusion.

The region $x/d < 2$ has been crosshatched in Figs. 3–5 to indicate that the data cannot be reliably obtained this close to the base from the present streak photographs because of overexposure and rapid deceleration.

Slattery and Clay[1] measured wake velocities of 12.5° θ_c cones by following packages of density gradients in schlieren motion pictures from frame to frame. The initial values of V_{wake}/V_{body} determined by Slattery and Clay, $V_{wake}/V_{body} = 0.20$ at $x/d \approx 60$, are somewhat higher than the final value $V_{wake}/V_{body} \approx 0.1$ at $x/d = 22$ reported here. The difference is believed to be due to the relatively long shutter speed of the Fastax camera used for observing wake flow velocities in this region of the wake. The accuracy of their technique improves for $x/d > 100$, where the wake speeds are slower.[9]

References

[1] Slattery, R. E. and Clay, W. G., "The turbulent wake of hypersonic bodies," ARS Preprint 2673-62 (1962).

[2] Hromas, L. and Lees, L., "Effect of nose bluntness on the turbulent hypersonic wake," Space Technology Labs. Rept. 6130-6259-KU-000 (October 1962).

[3] Webb, W. H., private communication (September 1963).

[4] Lien, H., Erdos, J., and Pallone, A., "Nonequilibrium wakes with laminar and turbulent transport," AIAA Preprint 63-447 (1963).

[5] Hidalgo, H., Taylor, R. L., and Keck, J. C., "Transition in the viscous wake of blunt bodies at hypersonic speeds," Avco-Everett Research Lab. Res. Rept. 133 (April 1961); also J. Aerospace Sci. **29**, 1306–1316 (1962).

[6] Lien, H., private communication (September 1963).

[7] Fay, J. and Goldburg, A., "Unsteady hypersonic wake behind blunt bodies," AIAA J. **1**, 2264–2272 (1963); also "The unsteady hypersonic wake behind spheres," Avco-Everett Research Lab. Res. Rept. 139 (November 1962).

[8] Goldburg, A., "Analysis of hypersonic wake transition experiments," Avco-Everett Research Lab. Res. Rept. (to be published).

[9] Slattery, R., private communication (October 1963).

Pressure Gradients in a Liquid Propellant Rocket Motor

WILLIAM T. PESCHKE* AND SANFORD S. HAMMER†
Polytechnic Institute of Brooklyn, Farmingdale, N. Y.

Introduction

IN the design of liquid propellant rocket combustors it is desired to have complete burning take place within the combustion chamber. In addition, the liquid- and gasdynamic flow fields should be inherently stable. Recent investigations,[1, 2] based on a vaporization rate controlled combustion process, resulted in methods to determine the minimum chamber length required to insure complete combustion and the flow fields response to input disturbances. The theoretical analysis predicted mass liberation schedules, gas and droplet velocity histories, and axial pressure histories. It was found that increases in the mass liberation rate are accompanied by attendant increases in the magnitude of the pressure gradient with a corresponding increase in the velocity gradient. Initial experiments designed to measure axial pressure gradients were in good agreement with the theory for a given set of injection parameters.[1] In order to obtain correlation, it was necessary to assume a drop size distribution and a droplet formation distance, i.e., the required distance from the injector face for the injected ligaments to form a discrete droplet distribution. The analysis distinctly indicated that energy (mass) liberation gradients can be deduced from pressure gradient measurements. Thus, the chamber length for optimum propellant utilization and thrust production is related to the axial pressure gradient. In a motor whose geometry and propellant mass flow rate are fixed, this gradient

Received March 25, 1964; revision received May 1, 1964. The results obtained in this paper were obtained in the course of research sponsored by the Air Force Office of Scientific Research under Grant No. AF-AFOSR-86-63. The authors wish to acknowledge Vito D. Agosta for his helpful discussions.

* Research Assistant, Aerospace Engineering, Propulsion Research Laboratory. Member AIAA.

† Research Associate, Aerospace Engineering, Propulsion Research Laboratory. Member AIAA.

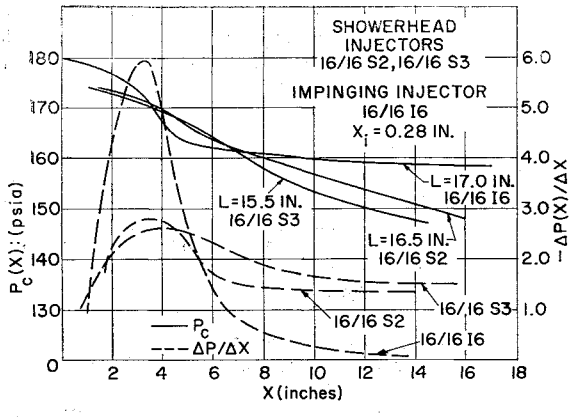

Fig. 1 Axial pressure variation and gradient for showerhead and impinging injectors.

is almost entirely dependent on the nature of the injection process.

In addition, the behavior of an input pressure disturbance is dependent on the gasdynamic velocity field through which the disturbance propagates. Thus, the characteristic gradients or signatures produced by various injectors are important parameters in determining the stability or instability of a thrust chamber system.

Experimental Equipment

A rocket engine of 500 lbf nominal thrust, consisting of an injector, uncooled brass cylindrical chamber, and a converging-diverging nozzle in separable units is employed. The chamber length can be varied between 8 and 24 in., although all of the data reported here are for 17-in. chambers except where noted. The chamber and nozzle throat diameters are 2 and 1.65 in., respectively, resulting in a contraction ratio of 1.47. This yields a high nozzle entrance Mach number 0.45, which was verified experimentally. The propellants are JP-5A and liquid oxygen.

All of the injectors used in the investigation contain 16 fuel and oxidizer orifices. The oxidizer orifice is maintained constant at 0.0595-in. diam, and the fuel orifices are 0.042-in. diam, except in the second showerhead injector, which has multisized orifices in order to obtain a greater distribution of fuel droplets. All impinging injectors are of the unlike-impinging stream pattern type, i.e., fuel on oxidizer.

Eight pressure ports in the chamber are connected to a single pressure transducer through a commutating system. A piezoelectric crystal transducer (Kistler PZ-14) is used to sense the pressure difference from port to port. A reference absolute chamber pressure is measured with a transducer mounted in the rocket motor wall. The transducer outputs are recorded on a light beam-galvanometer oscillograph.

In order to eliminate the effects of injection velocity on the droplet ballistics and subsequent evaporation history, the total liquid propellant mass flow, oxidizer-fuel ratio, and total injection area of both JP-5A and liquid oxygen are held constant throughout the series of tests presently reported. JP-5A injection velocity is 85 fps. The average total propellant flow is 2.35 lbm/sec at an O/F ratio of 2.62. A 5% variation from the average flow rate is allowed for inclusion in the test results.

Discussion of Results

The data for the injectors tested are presented both as pressure vs axial distance and pressure gradient ($\Delta P/\Delta x$) vs the average axial distance over which the gradient was computed. It should be noted that later tests included a static pressure tap at the injector face. Consequently, the more recent data presented includes a pressure measurement at this point.

Figure 1 shows the data for two showerhead injectors and one impinging injector. The two showerheads both contain four alternating rings of fuel and oxidizer, but differ in fuel orifice diameter. The S2 injector contains sixteen 0.042-in.-diam orifices whereas the S3 has eight 0.035-in.-, four 0.043-in.-, and four 0.052-in.-diam orifices. The impinging injector was designed for an impingement distance (x_i) of 0.28 in. The data indicate a much steeper gradient and, hence, a more localized region of evaporation and combustion for the impinging injector than for either of the showerheads. The use of multisized orifices results in a more uniform pressure gradient and hence a spreading of the evaporation and combustion zone.

Data for a radial sheet and tangential sheet impinging injector with the same design impingement distance are shown in Fig. 2. Both injectors contain the same number and size of orifices. The tangential sheet injector contains a single ring of doublets, whereas the radial sheet injector contains two rings of doublets. The latter injector increases mixing and atomization of the fuel and oxidizer and results in more rapid utilization of the propellants. Thus, the maximum point on the pressure gradient curve for the radial sheet injector is closer to the injector face than the corresponding point for the tangential sheet injector. This indicates that the main evaporation and combustion zone has been shifted upstream with the I2 injector and implies that a shorter chamber would be required to obtain maximum propellant evaporation.

The results obtained with two additional impinging injectors, each of which contains three impingement distances, are shown in Fig. 3 together with the single impingement point, I6 injector. As the impingement point is moved downstream, the degree of mixing decreases and the evaporation and combustion zone is spread out over a greater axial distance. The high amplitude and thin width of the pressure gradient peak

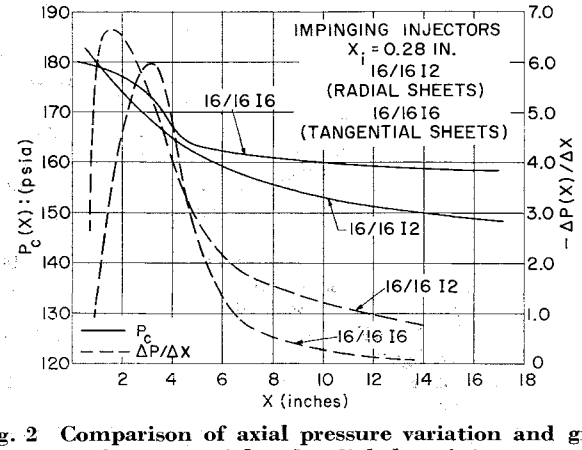

Fig. 2 Comparison of axial pressure variation and gradient for tangential and radial sheet injectors.

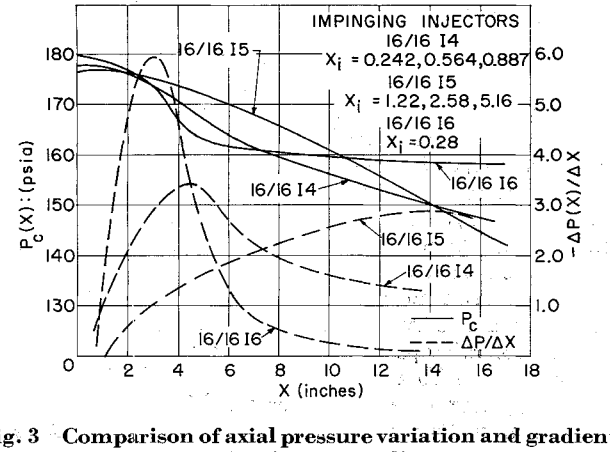

Fig. 3 Comparison of axial pressure variation and gradient for various impingement distances.

for the I6 injector indicate a zone of high evaporation and combustion approximately 4 in. from the injector face. The injector with impingement distances less than 1 in. has a peak in the pressure gradient curve 6 in. from the injector face, whereas the pressure gradient for the last injector indicates a peak near the nozzle entrance. This implies a high degree of evaporation and gas generation in the downstream portions of the chamber.

Data have recently been obtained from three tangential sheet impinging injectors with design impingement points greater than 1 in. Although it cannot be readily determined whether or not impingement takes place at such large distances from the face, the data indicate that, as the intended impingement point is moved downstream, the rate of pressure drop decreases. At the maximum impingement distance tested, the effect of poorer mixing and low propellant utilization is evidenced by the decrease in over-all chamber pressure, despite a somewhat higher propellant flow rate.

The performance with this last injector (I9) is inferior to that obtained with the showerhead S2 injector discussed previously. Aside from the obvious differences between the two injectors, the showerhead contains four alternating rings of fuel and oxidizer, whereas the impinging injector contains a single ring of doublets. It appears then that distribution of the propellant over a greater portion of the chamber cross section enhances mixing and atomization and promotes the evaporation process. Tests conducted with a two-ring showerhead indicate that a chamber length of 21 in. is required for optimum performance, whereas the four-ring injector only required 14 in.

The three injectors just discussed are equipped with pressure taps in the injector face. The data show that the point of maximum chamber pressure is downstream from the injector face, and the pressure gradient near the face is positive. This is indicated by a negative value of $-(\Delta P/\Delta x)$. This suggests the existence of a recirculation zone or negative velocity gradient in the region near the injector face.

Conclusions

Variations in injector configuration produce variations in axial pressure history in a constant area liquid propellant rocket motor. These pressure variations are due to changes in the mixing and shattering characteristics of different injectors and are concurrent with unique evaporation and mass liberation profiles. For an injector that promotes rapid droplet breakup and intimate mixing of propellants, such as the I6 used in these experiments, the chamber pressure has a maximum gradient close to the injector face with a correspondingly high gas acceleration. This action exerts additional gasdynamic effects on the unconsumed droplets, enhancing propellant consumption.

Since the attenuation or amplification of a pressure wave is dependent on the gasdynamic field through which it propagates, the inherent stability or instability of an injector-chamber system is keyed to the pressure-velocity gradient produced.

In addition, the data can be used to establish design criteria for steady-state operation and to predict critical conditions that can exist because of large pressure gradients that result in high heat-transfer rates to the injector face or rocket chamber wall.

References

[1] Burstein, S., Hammer, S., and Agosta, V., "Spray combustion model with droplet breakup: analytical and experimental results," *ARS Progress in Astronautics and Rocketry: Detonation and Two-Phase Flow*, edited by S. S. Penner and F. A. Williams (Academic Press, New York, 1962), Vol. 6, pp. 243–267.

[2] Burstein, S. and Agosta, V., "Combustion instability: Nonlinear analysis of wave propagation in a liquid propellant rocket motor," Polytechnic Institute of Brooklyn, Propulsion Research Lab. Rept. 62-15, AD 282 970 (March 1962).

Euler Angles for Libration Analysis

IRVING MICHELSON*
Illinois Institute of Technology, Chicago, Ill.

INCREASINGLY stringent satellite attitude stability requirements have necessitated accurate dynamical descriptions of librational motion consisting of limited angular displacements about satellite centroid. Although Euler's angle convention has always been followed in treatises on dynamics of rotating bodies, it introduces a peculiar inconvenience in discussions of librations: small angular displacements of arbitrary direction cannot be represented by a set of small values of the Eulerian angles. Although quaternions or different angle conventions could be introduced which are not subject to this disadvantage, there is an understandable reluctance to adopt these, owing to the attendant loss of accessibility to the classic literature and methods which this would entail. It is shown below that sets of finite Euler angles can be found which possess all of the properties desired for treating general librational motions, thus obviating the necessity for introduction of unconventional analytical techniques.

The need for a convention for representing angular displacements is recalled to be a consequence of the fact that these are not vector quantities, since magnitude, direction, and also sequence determine the resultant of two or more rotations; i.e., angular displacements do not enjoy the commutative property of addition. Among the many ways of securing an arbitrary rotation by compounding rotations about a set of orthogonal directions, Euler's convention, being adequate, has long held universal acceptance. A rotation ψ about one axis X, followed by a rotation θ about a perpendicular axis Y, and a final rotation φ about the original axis bring the axes to positions x, y. The two right-handed triads X, Y, Z and x, y, z are then related by equations compactly expressed in matrix form[1]:

$$\begin{bmatrix} x \\ x \\ z \end{bmatrix} = \begin{bmatrix} \cos\theta & \sin\psi\sin\theta & -\cos\psi\sin\theta \\ \sin\theta\sin\varphi & \cos\psi\cos\varphi - \sin\psi\cos\theta\sin\varphi & \sin\psi\cos\varphi + \cos\psi\cos\theta\sin\varphi \\ \sin\theta\cos\varphi & -\cos\psi\sin\varphi - \sin\psi\cos\theta\cos\varphi & -\sin\psi\sin\varphi + \cos\psi\cos\theta\cos\varphi \end{bmatrix} \cdot \begin{bmatrix} X \\ Y \\ Z \end{bmatrix} \quad (1)$$

Although zero displacements Ψ, θ, φ clearly do reduce the transformation matrix to unit diagonal form, it is also seen directly that first-order small values of these angles do not correspond to a rotation of arbitrary direction. For this purpose, it is sufficient to compare (1) with the transformation that corresponds to infinitesimal rotations α, β, γ about axes X, Y, Z, as done in librations analysis[2]:

$$\begin{bmatrix} x \\ y \\ z \end{bmatrix} = \begin{bmatrix} 1 & \gamma & -\beta \\ -\gamma & 1 & \alpha \\ \beta & -\alpha & 1 \end{bmatrix} \cdot \begin{bmatrix} X \\ Y \\ Z \end{bmatrix} \quad (2)$$

Note in particular that the matrix element $\sin\psi\sin\theta$ vanishes to the second order in the Eulerian transformation (1), whereas the corresponding Z rotation γ in (2) is only first-order small. Hence, small values of the Euler angles do not represent small rotations that have a Z component. The geometrical reason for this is to be found in the unsymmetrical character of Euler's convention: two rotations about X, one about Y, and none about Z. The more symmetrical rotation sequence that leads to the transformation (2), on the other hand, entails exactly one rotation about each of three axes and thus is of a different class from Euler's, the same being true of course when the angles α, β, γ are finite and arranged in a definite sequence.

Received March 25, 1964.

* Professor of Aerospace Engineering, Department of Mechanical and Aerospace Engineering. Member AIAA.